Title	Relationship between Local Structure and Oxide Ionic Diffusion of Nd[2]NiO[4+ δ] with K[2]NiF[4] Structure
Author(s)	INA, Toshiaki; ORIKASA, Yuki; MASESE, Titus; NAKAO, Takayuki; MINESHIGE, Atsushi; AMEZAWA, Koji; TANIDA, Hajime; URUGA, Tomoya; UCHIMOTO, Yoshiharu
Citation	Electrochemistry (2014), 82(10): 875-879
Issue Date	2014-10
URL	http://hdl.handle.net/2433/191121
Right	© 2014 The Electrochemical Society of Japan
Type	Journal Article
Textversion	author

Relationship between Local Structure and Oxide Ionic Diffusion of $Nd_2NiO_{4+\delta}$ with K_2NiF_4 Structure

Toshiaki INA[a], Yuki ORIKASA[a,] *, Titus MASESE[a], Takayuki NAKAO[a], Atsushi MINESHIGE[b], Koji AMEZAWA[c], Hajime TANIDA[d], Tomoya URUGA[d], Yoshiharu UCHIMOTO[a]

[a] Graduate School of Human and Environmental Studies, Kyoto University, Yoshida-nihonmatsu-cho, Sakyo-ku, Kyoto 606-8501 Japan

[b] Graduate School of Engineering, University of Hyogo, 2167 Shosha, Himeji 671-2280, Japan

[c] Institute of Multidisciplinary Research for Advanced Materials, Tohoku University, 2-1-1Katahira, Aoba-ku, Sendai, Miyagi 980-8577, Japan

[d] Japan Synchrotron Radiation Research Institute (JASRI), 1-1-1, Kouto, Sayo-cho, Sayo-gun, Hyogo 679-5198, Japan

**Corresponding author; orikasa.yuuki.2a@kyoto-u.ac.jp*

Abstract

The relationship between the local structure and oxide ionic conduction of $Nd_2NiO_{4+\delta}$ possessing the K_2NiF_4 structure was investigated. Various oxygen nonstoichiometry samples of $Nd_2NiO_{4+\delta}$ prepared with different annealing oxygen partial pressures were examined. The local structure related to oxide ionic conduction was determined by the Nd *K*-edge extended X-ray absorption fine structure. The oxide ionic conductivity and surface exchange coefficient were estimated using electronic conductivity relaxation methods. The activation energy for the oxide ionic conductivity was found to have a direct correlation to the surface exchange coefficient. The bottleneck size for oxide ion conduction was strongly correlated to the oxide ionic conduction of interstitial oxygen and the oxygen surface exchange rate.

Keywords: Oxide ion conduction, Nd_2NiO_4, Local structure, Extended X-ray absorption fine structure

1. Introduction

K_2NiF_4-type lanthanum, neodymium and/or praseogymium nickelates, $Ln_2NiO_{4+\delta}$ (Ln = La, Nd, or Pr), show mixed oxide ionic and electronic conductivities[1-7]. Because of their mixed conduction properties, $Ln_2NiO_{4+\delta}$ have attracted attention as cathode materials for solid oxide fuel cells (SOFCs)[8, 9]. Furthermore, the thermal expansion coefficients of Ln_2NiO_4-based materials are comparable to those of doped ceria and lanthanum gallate, which are well-known solid electrolytes[6, 10-13]. The cathode of SOFCs should have high oxygen reduction kinetics, which, in turn, should depend on the oxide ionic diffusion and oxygen surface exchange rate[14]. Although the oxygen self-diffusion coefficient of $Ln_2NiO_{4+\delta}$ has been reported by various researchers, there are discrepancies in the reported values[15-19]. In order to design electrode materials that show a good electrochemical property, it is important to investigate the factors determining the oxide ionic diffusion.

Previous studies revealed that $Ln_2NiO_{4+\delta}$ show anisotropic oxide ion conduction[16, 18, 20-22]. The principle mechanism for oxide ion diffusion is considered to involve ionic hopping between interstitial oxygen sites located in alternate LnO rock salt layers along the *ab* plane of the structure[18, 22]. Any possible path for oxygen diffusion along the *c* axis involves less favorable diffusion through fully occupied

oxygen sites in the perovskite blocks. The reported diffusion coefficient along the *c* axis can be several orders of magnitude lower than that for the *ab* plane[15, 16]. The introduction of interstitial oxygen during oxide ionic diffusion causes a local structural change around the hopping oxygen site. A local structural analysis can provide important information about the oxide ionic diffusion mechanism.

Information from X-ray absorption spectroscopy (XAS) is useful for the analysis of the local structural changes generated around the oxygen point defect structure. We previously reported the results of electronic and local structural analyses of simple perovskite-type oxides with oxygen deficient structures[23-25]. However, only a few reports investigated the local structural analyses related to oxide ionic diffusion in an interstitial oxygen $Ln_2NiO_{4+\delta}$ system.

In this study, we prepared $Nd_2NiO_{4+\delta}$ samples with various amounts of interstitial oxygen as model samples and clarified the local structural changes with the introduction of interstitial oxygen by employing XAS. The oxygen surface exchange coefficient and oxide ionic conductivity in $Nd_2NiO_{4+\delta}$ were investigated by using the electronic conductivity relaxation method[26]. We discussed the local structural factors that govern the oxygen surface exchange coefficient and oxide ionic conductivity in $Nd_2NiO_{4+\delta}$.

2. Experimental

$Nd_2NiO_{4+\delta}$ was synthesized through a conventional solid-state reaction[27]. In brief, stoichiometric amounts of Nd_2O_3 (Kojundo Chemical), predried in air at 1273 K, and NiO (Wako Pure Chemical) were weighed and pulverized. A calcining process was performed at 1273 K for 10 h. The obtained $Nd_2NiO_{4+\delta}$ powders were pressed into pellets and sintered at 1573 K in air for 10 h. The sintered pellets were annealed at 1073 K for 4 h under the desired oxygen partial pressure ($p(O_2)$). The oxygen partial pressure was maintained at 10^5, 10^4, 10^3, 10^2, or 10^1 Pa by purging high-purity O_2 or Ar/O_2 gas mixtures. After annealing, the pellets were quenched to room temperature while maintaining the oxygen partial pressure. All the annealed samples were characterized by powder X-ray diffraction (XRD) using Cu-$K\alpha$ radiation (RIGAKU, RINT2200) for phase identification. The diffraction patterns were recorded in the 2θ range 10°–80° in 0.02° steps. All the patterns were fully indexed to an *Fmmm* space group with the orthorhombic K_2NiF_4 structure. The XRD patterns contained no impurities, which indicated that all the samples used in this study were single-phase K_2NiF_4-type compounds. The lattice constant was calculated. The oxygen content of each sample was determined using iodometric titration[28].

XAS measurements at the Nd *K*-edge were performed at beamline BL01B1 of SPring-8 at the Japan Synchrotron Radiation Research Institute (JASRI) in Sayo, Japan. The Nd *K*-edge spectra were measured in the transmission mode using a Si(311) monochromator at room temperature. The samples were prepared by grinding the $Nd_2NiO_{4+\delta}$ with boron nitride (BN) and then compressing to obtain homogeneous samples. The REX2000 data analysis software (Rigaku Corp.) was used to evaluate the extended X-ray absorption fine structure (EXAFS) data. In these EXAFS analyses, the oscillation was first extracted from the EXAFS data by using a spline smoothing method[29]. For the Fourier transformation, the spectra in the range $3.650 \leq k \leq 12.55$ Å^{-1} were weighed using a Hanning window. The theoretical scattering phase shifts and amplitudes were calculated using FEFF8.20[30].

Electrical conductivity relaxation (ECR) measurements were performed over the $p(O_2)$ range 10^1–10^5 Pa within 873–1173 K. A $Nd_2NiO_{4+\delta}$ sample (about 2.2 × 2.2 × 12 mm^3) wired with platinum at four points was set in a quartz tube. The sample temperature and $p(O_2)$ were measured using an R-type thermocouple and YSZ oxygen sensor placed close to the sample, respectively. Four-point dc conductivity relaxation measurements were conducted by changing the gas mixing ratio while recording the transient voltage signal as a function of time. The time dependency of the electrical

conductivity, σ(t)-σ(0)/σ(∞)-σ(0), was plotted and fitted to the theoretical equation outlined in the literature[31]. The chemical surface exchange coefficient (k_{chem}) and chemical diffusion coefficient (D_{chem}) were evaluated using ECR, and the oxygen surface exchange coefficient oxide (k_O) and ionic conductivity (σ_i) were calculated from the results of k_{chem}, D_{chem}, and oxygen nonstoichiometry.

3. **Results and Discussion**

The various $p(O_2)$ values for annealing produced different oxygen nonstoichiometry samples of $Nd_2NiO_{4+\delta}$. Figure 1 shows the oxygen nonstoichiometry of $Nd_2NiO_{4+\delta}$ calculated from the mean valence of Ni obtained by iodometric titration assuming the presence of trivalent Nd ions. These values are in good agreement with the reported values[11]. For the entire range of $p(O_2)$ values, $Nd_2NiO_{4+\delta}$ exhibited oxygen-excess compositions. The amount of excess oxygen in $Nd_2NiO_{4+\delta}$ increased with increasing $p(O_2)$. The change in the nonstoichiometry for $Nd_2NiO_{4+\delta}$ can be expressed in terms of the defect equilibrium using the following Kröger–Vink notation:

$$\mathrm{Ni}_{\mathrm{Ni}}^{\times} + \frac{1}{2}V_i^{\times} + \frac{1}{4}\mathrm{O}_2(g) \overrightarrow{\leftarrow} \mathrm{Ni}_{\mathrm{Ni}}^{\bullet} + \frac{1}{2}\mathrm{O}_i'' \qquad (1)$$

where $\mathrm{Ni}_{\mathrm{Ni}}^{\times}$ is a nickel ion on a nickel site with neutral charge, $\mathrm{Ni}_{\mathrm{Ni}}^{\bullet}$ is a nickel ion on a nickel site with a positive charge, $V_i^{\times}$ is a vacancy on an interstitial site with neutral

charge, O_i'' is an oxygen ion on an interstitial site with two negative charges, and $O_2(g)$ is an oxygen molecule in the gas phase. This means that, for $Nd_2NiO_{4+\delta}$, the valence state of Ni and the amount of excess oxygen increases as $p(O_2)$ increases.

In order to reveal the local structural changes in the rock salt layer because of the introduction of interstitial oxide ions, the Nd *K*-edge EXAFS was applied to $Nd_2NiO_{4+\delta}$. Figure 2 shows the Fourier transforms of the k^3-weighed EXAFS oscillation at the Nd *K*-edge of $Nd_2NiO_{4+\delta}$ annealed at 1073 K under various $p(O_2)$ values. The first peak at ~2Å is a signal from the nearest coordination Nd-O shells, the second peak at 2–3 Å arises from the second nearest coordination Nd-Ni shells, and the third peak at 3–4 Å is a signal from the third nearest coordination Nd-Nd shells. Every peak intensity increases and shifts toward the longer interatomic distance with increasing $p(O_2)$. This trend indicates that the local distortion in the coordination shells decreases when the interatomic distance increases. To obtain quantitative information, curve fittings were performed in the *k* space. The following equation was used for these fittings:

$$\chi(k) = \sum_i \frac{N\left|f(k,\pi)\right|\exp(-2W_i^2k^2)\exp(-2\frac{R_i}{\lambda_i})\sin\left[2k\,R_i+\phi_i(k)\right]}{k\,R_i^2} \quad (2)$$

where χ is the oscillation in the *k* space, *N* is the coordination number, $f(k,\pi)$ is the backscattering amplitude, W_i is the Debye–Waller (DW) factor, R_i is the interatomic

distance, λ_i is the mean free path, and φ_i is the phase shift of the photoelectrons. Table 1 lists the EXAFS structural parameters taken at the Nd *K*-edge obtained by the fitting procedure for the experimental $k^3\chi(k)$ at Nd-O1, Nd-O2, Nd-O3, Nd-Ni, Nd-Nd1, and Nd-Nd2 distances (*R*) and the DW factor (*W*) for $Nd_2NiO_{4+\delta}$ annealed under various oxygen partial pressures at 1073 K. The residual errors (R_s), as determined by

$$R_s = \frac{\sum\left\{k^3\chi_{obs}(k) - k^3\chi_{cal}(k)\right\}^2}{\sum\left\{k^3\chi_{obs}(k)\right\}^2} \quad (3)$$

are subtle, as is apparent in Table 1, unambiguously indicating that accurate fittings were performed in this study. The local structure coordination for the EXAFS analysis around the Nd atom in the $Nd_2NiO_{4+\delta}$ crystal structure is provided in Fig. 3 (a). Nd-O1, Nd-O2, and Nd-O3 represent the axial coordination along the rock salt layer, equatorial coordination, and other coordination, respectively. Nd-Nd1 represents the axial coordination along the perovskite structure, while Nd-Nd2 represents the equatorial coordination. These local structure parameters will be discussed in a later section.

For the ionic diffusion path in solid-state materials, there is a bottleneck for the diffusion, which is expressed by the energetic saddle point of the migration. The mechanism for the interstitial oxygen migration of the K_2NiF_4 structure was reported to be *interstitially* migration[18, 22, 32]. Figure 3 (b) shows a schematic illustration of the

interstitial oxygen diffusion for $Nd_2NiO_{4+\delta}$. The interstitial oxide ion moves toward the apical oxygen of the NiO_6 octahedron, and then the apical oxygen moves to another interstitial site. The green triangle comprising three Nd atoms represents the bottleneck for interstitial oxygen migration[22]. In order to estimate the size of this bottleneck, the interatomic distances of Nd-Nd1 and Nd-Nd2 are important.

Figure 4 shows the dependence of the distances of the Nd-Nd1 and Nd-Nd2 pairs of $Nd_2NiO_{4+\delta}$ annealed under various $p(O_2)$ values at 1073 K obtained from the EXAFS analysis. As $p(O_2)$ increases, the Nd-Nd1 distance increases. This result shows that the introduction of interstitial oxygen in the rock salt layer produces an expansion of the perovskite structure. This is consistent with the expansion of the *c*-axis length with the introduction of interstitial oxygen[11]. There is almost no change in the variation of the Nd-Nd2 distance with the introduction of an interstitial oxide ion. This result shows that the base of the bottleneck triangle does not change with the introduction of an interstitial oxide ion.

In order to quantitatively discuss the oxygen migration mechanism of $Nd_2NiO_{4+\delta}$, the oxide ionic conductivity and oxygen exchange coefficient were calculated using the following equation,

$$\sigma_i = \frac{4F^2 c_i D_O}{RT} \quad (4)$$

where σ_i is the oxide ionic conductivity, F is the Faraday constant, c_i is the molar concentration of interstitial oxide ions, D_O is the self-diffusion coefficient of oxygen, R is the ideal gas constant, and T is temperature[26]. D_O and the oxygen surface exchange coefficient k_O are related to the chemical diffusion coefficient D_{chem} and the chemical surface exchange coefficient k_{chem} via a thermodynamic factor of oxygen γ_o[33],

$$\gamma_O = \frac{1}{2}\frac{\partial \ln pO_2}{\partial \ln c_O} = \frac{D_{chem}}{D_O} = \frac{k_{chem}}{k_O} \quad (5)$$

where c_o is the molar concentration of oxide ions[26]. In order to calculate γ_o, c_o is needed, which is calculated using the nonstoichiometric data for $Nd_2NiO_{4+\delta}$ reported by Nakamura *et al.*[11, 34] In addition to the bulk conductivity, the contribution of the grain boundary to the conductivity should be considered. However, the conductivity relaxation profiles are well fitted by using a single relaxation process, and the experimental data are consistent with the previously reported D_O in bulk[35]. Therefore, the contribution of the grain boundary to the conductivity is negligibly small and the oxide ionic conductivity arises from the bulk conductivity.

Figure 5 shows the oxide ionic conductivity (σ_i) and oxygen surface exchange coefficient (k_O) of $Nd_2NiO_{4+\delta}$ under various oxygen partial pressures as a function of temperature. The σ_i and k_O values of $Nd_2NiO_{4+\delta}$ represent an Arrhenius-type behavior

for various oxygen partial pressures. To better understand this trend, a comparison is made between the activation energies for σ_i and k_O. Figure 6 shows the activation energy for the k_O of $Nd_2NiO_{4+\delta}$ as a function of activation energy for σ_i; both the activation energies are linearly correlated. The estimated activation energy for σ_i of $Nd_2NiO_{4+\delta}$ is 64-90 kJ mol^{-1} in this study, which is comparable to the reported values of $Nd_2NiO_{4+\delta}$ and $La_2NiO_{4+\delta}$[36-38]. The result in Fig. 6 shows that oxide ionic conduction governs the oxygen surface exchange coefficient in $Nd_2NiO_{+\delta}$. This result is similar to the relationship between the oxygen surface exchange coefficients and the oxygen tracer diffusion coefficient in simple perovskite oxides[39].

As mentioned earlier, the bottleneck for oxide ionic conduction consists of three Nd atoms (Fig. 3 (b)). In light of this, calculations were made using the *c*-axis length and Nd-Nd1 and Nd-Nd2 distances in order to obtain quantitative values for the bottleneck size using the following equations:

$$S = \frac{hL_{\mathrm{Nd-Nd2}}}{2} \tag{6}$$

$$h = \sqrt{\left(L_{\mathrm{Nd-Nd}}\right)^2 + \left(\frac{L_{\mathrm{Nd-Nd2}}}{2}\right)^2} \tag{7}$$

$$L_{\mathrm{Nd-Nd}} = \frac{c - 2L_{\mathrm{Nd-Nd1}}}{2} \tag{8}$$

where S, h, $L_{Nd\text{-}Nd}$, $L_{Nd\text{-}Nd1}$, $L_{Nd\text{-}Nd2}$, and c represent the bottleneck size, height of the bottleneck triangle, distance between the upper Nd sheet and lower Nd sheet in the rock salt layer, interatomic Nd-Nd1 distance, interatomic Nd-Nd2 distance, and lattice constant of the c axis, respectively. Figure 7 shows the activation energies of σ_i and k_O as a function of the bottleneck size of $Nd_2NiO_{4+\delta}$. The activation energies of σ_i and k_O increase when the bottleneck size decreases from 6.27 to 6.24 Å. This result shows that the governing factor for oxide ion diffusion is the bottleneck size for interstitial oxygen diffusion under a high oxygen partial pressure condition. However, the activation energies are almost constant below a bottleneck size of 6.24 Å, which corresponds to low oxygen partial pressures. The independence of the activation energy on the bottleneck size implies that another diffusion path such as the migration of oxygen vacancies in the perovskite layer is utilized, because the diffusion along the *ab* plane is disturbed. This hypothesis was demonstrated by a molecular dynamics study in an oxygen-deficient $La_{2-x}Sr_xCoO_4$ system[40]. The lower oxygen partial pressure may induce oxygen vacancies in the perovskite layers of $Nd_2NiO_{4+\delta}$. Recently, Yamada et al. reported that the anisotropic catalytic activity of the orientation controlled a $Nd_2NiO_{4+\delta}$ electrode, and the mechanical stress between the electrode and the electrolyte played an important role in the catalytic activity[8, 41]. Considering our results, the induced

mechanical stress might change the bottleneck size in $Nd_2NiO_{4+\delta}$, which would change the oxide ionic conduction and oxygen surface exchange kinetics. Adequately controlling the bottleneck size could improve the electrochemical properties of $Nd_2NiO_{4+\delta}$.

4. Conclusion

The relationship between the local structure and oxide ionic conduction of $Nd_2NiO_{4+\delta}$ possessing a K_2NiF_4 structure was investigated. The local structure related to oxide ionic conduction was determined using the Nd *K*-edge EXAFS. The oxide ionic conductivity and surface exchange coefficient were estimated using electronic conductivity relaxation methods. By comparing the bottleneck size and activation energies for the oxygen surface exchange coefficient and oxide ionic conductivity, a correlation was established between the activation energies and the bottleneck size. Adequately controlling the bottleneck size could improve cathode materials with the K_2NiF_4 structure and provide remarkable oxide ionic conductivity.

REFERENCES

1. V.V. Vashook, S.P. Tolochko, L. Yushkevich, L.V. Makhnach, I.F. Kononyuk, H. Altenburg, J. Hauck, H. Ullmann, *Solid State Ionics*, **110**, 245 (1998).

2. V.V. Kharton, A.P. Viskup, E.N. Naumovich, F.M.B. Marques, *J. Mater. Chem.*, **9**, 2623 (1999).

3. S.J. Skinner, J.A. Kilner, *Solid State Ionics*, **135**, 709 (2000).

4. G.Q. Wu, J.J. Neumeier, *Phys. Rev. B*, **67**, 125116 (2003).

5. E. Boehm, J.M. Bassat, P. Dordor, F. Mauvy, J.C. Grenier, P. Stevens, *Solid State Ionics*, **176**, 2717 (2005).

6. A. Aguadero, J.A. Alonso, M.J. Martinez-Lope, M.T. Fernandez-Diaz, M.J. Escudero, L. Daza, *J. Mater. Chem.*, **16**, 3402 (2006).

7. F. Mauvy, C. Lalanne, J.M. Bassat, J.C. Grenier, H. Zhao, L.H. Huo, P. Stevens, *J. Electrochem. Soc.*, **153**, A1547 (2006).

8. A.M. Hernandez, L. Mogni, A. Caneiro, *Int. J. Hydrogen Energy*, **35**, 6031 (2010).

9. M. Rieu, R. Sayers, M.A. Laguna-Bercero, S.J. Skinner, P. Lenormand, F. Ansart, *J. Electrochem. Soc.*, **157**, B477 (2010).

10. T. Nakamura, K. Yashiro, K. Sato, J. Mizusaki, *Solid State Ionics*, **181**, 292 (2010).

11. T. Nakamura, K. Yashiro, K. Sato, J. Mizusaki, *Solid State Ionics*, **181**, 402 (2010).

12. V.V. Kharton, F.M. Figueiredo, L. Navarro, E.N. Naumovich, A.V. Kovalevsky, A.A. Yaremchenko, A.P. Viskup, A. Carneiro, F.M.B. Marques, J.R. Frade, *J. Mater. Sci.*, **36**, 1105 (2001).

13. V.V. Kharton, A.L. Shaula, N.P. Vyshatko, F.M.B. Marques, *Electrochim. Acta*, **48**, 1817 (2003).

14. S.B. Adler, *Chem. Rev.*, **104**, 4791 (2004).

15. J.M. Bassat, P. Odier, A. Villesuzanne, C. Marin, M. Pouchard, *Solid State Ionics*, **167**, 341 (2004).

16. M. Burriel, G. Garcia, J. Santiso, J.A. Kilner, J.C.C. Richard, S.J. Skinner, *J. Mater. Chem.*, **18**, 416 (2008).

17. A.R. Cleave, J.A. Kilner, S.J. Skinner, S.T. Murphy, R.W. Grimes, *Solid State Ionics*, **179**, 823 (2008).

18. A. Chroneos, D. Parfitt, J.A. Kilner, R.W. Grimes, *J. Mater. Chem.*, **20**, 266 (2010).

19. R. Sayers, R.A. De Souza, J.A. Kilner, S.J. Skinner, *Solid State Ionics*, **181**, 386 (2010).

20. G. Kim, S. Wang, A.J. Jacobson, C.L. Chen, *Solid State Ionics*, **177**, 1461 (2006).

21. S.J. Skinner, *Solid State Sci.*, **5**, 419 (2003).

22. M. Yashima, N. Sirikanda, T. Ishihara, *J. Am. Chem. Soc.*, **132**, 2385 (2010).

23. Y. Orikasa, T. Ina, T. Nakao, A. Mineshige, K. Amezawa, M. Oishi, H. Arai, Z. Ogumi, Y. Uchimoto, *J. Phys. Chem. C*, **115**, 16433 (2011).

24. Y. Orikasa, T. Ina, T. Nakao, A. Mineshige, K. Amezawa, M. Oishi, H. Arai, Z. Ogumi, Y. Uchimoto, *Phys. Chem. Chem. Phys.*, **13**, 16637 (2011).

25. Y. Orikasa, T. Nakao, M. Oishi, T. Ina, A. Mineshige, K. Amezawa, H. Arai, Z. Ogumi, Y. Uchimoto, *J. Mater. Chem.*, **21**, 14013 (2011).

26. A. Egger, E. Bucher, W. Sitte, *J. Electrochem. Soc.*, **158**, B573 (2011).

27. H. El Shinawi, C. Greaves, *J. Mater. Chem.*, **20**, 504 (2010).

28. J.W. Murray, L.S. Balistrieri, B. Paul, *Geochim. Cosmochim. Acta*, **48**, 1237 (1984).

29. J.W. Cook, D.E. Sayers, *J. Appl. Phys.*, **52**, 5024 (1981).

30. J.J. Rehr, J.M. Deleon, S.I. Zabinsky, R.C. Albers, *J. Am. Chem. Soc.*, **113**, 5135 (1991).

31. I. Yasuda, M. Hishinuma, *Solid State Ionics*, **80**, 141 (1995).

32. A. Kushima, D. Parfitt, A. Chroneos, B. Yildiz, J.A. Kilner, R.W. Grimes, *Phys. Chem. Chem. Phys.*, **13**, 2242 (2011).

33. J.E. ten Elshof, M.H.R. Lankhorst, H.J.M. Bouwmeester, *J. Electrochem. Soc.*, **144**, 1060 (1997).

34. T. Nakamura, K. Yashiro, K. Sato, J. Mizusaki, *J. Solid State Chem.*, **182**, 1533 (2009).

35. J.M. Bassat, M. Burriel, O. Wahyudi, R. Castaing, M. Ceretti, P. Veber, I. Weill, A. Villesuzanne, J.C. Grenier, W. Paulus, J.A. Kilner, *J. Phys. Chem. C*, **117**, 26466 (2013).

36. F. Mauvy, J.M. Bassat, E. Boehm, J.P. Manaud, P. Dordor, J.C. Grenier, *Solid State Ionics*, **158**, 17 (2003).

37. J.B. Smith, T. Norby, *J. Electrochem. Soc.*, **153**, A233 (2006).

38. A.L. Shaula, E.N. Naumovich, A.P. Viskup, V.V. Pankov, A.V. Kovalevsky, V.V. Kharton, *Solid State Ionics*, **180**, 812 (2009).

39. R.A. De Souza, J.A. Kilner, *Solid State Ionics*, **126**, 153 (1999).

40. C. Tealdi, C. Ferrara, P. Mustarelli, M.S. Islam, *J. Mater. Chem.*, **22**, 8969 (2012).

41. A. Yamada, Y. Suzuki, K. Saka, M. Uehara, D. Mori, R. Kanno, T. Kiguchi, F. Mauvy, J.C. Grenier, *Adv Mater*, **20**, 4124 (2008).

TABLE:

Table 1 Refined structural parameters of Nd *K*-edge EXAFS spectra for $Nd_2NiO_{4+\delta}$ annealed under various oxygen partial pressures. Distance (*R*) and Debye-Waller factor (σ) of Nd-O1, Nd-O2, Nd-O3, Nd-Ni, Nd-Nd1, and Nd-Nd2 are refined. Nd-O1 represents the axial coordination along the rock salt layer, Nd-O2 represents the equatorial coordination, and Nd-O3 represents the other coordination. Nd-Nd1 represents the axial coordination along the perovskite structure, while Nd-Nd2 represents the equatorial coordination.

$Nd_2NiO_{4+\delta}$	δ	Nd-O1(CN=1)		Nd-O2(CN=4)		Nd-O3(CN=4)		Nd-Ni(CN=4)	
Log[p (O_2)/Pa]		R / Å	W / Å	R / Å	W / Å	R / Å	W / Å	R / Å	W / Å
1	0.114	2.319(24)	0.063(37)	2.530(35)	0.099(35)	2.803(30)	0.108(31)	3.172(13)	0.127(18)
2	0.119	2.318(30)	0.074(39)	2.549(45)	0.109(42)	2.834(34)	0.110(37)	3.174(10)	0.115(13)
3	0.135	2.322(28)	0.069(38)	2.555(42)	0.106(41)	2.837(33)	0.112(38)	3.178(10)	0.112(11)
4	0.143	2.330(31)	0.074(40)	2.580(53)	0.116(53)	2.862(41)	0.116(43)	3.184(10)	0.109(10)
5	0.181	2.348(31)	0.076(45)	2.602(67)	0.125(69)	2.890(48)	0.116(45)	3.200(10)	0.105(10)

$Nd_2NiO_{4+\delta}$	δ	Nd-Nd1(CN=4)		Nd-Nd2(CN=4)		Residue
Log[p (O_2)/Pa]		R / Å	W / Å	R / Å	W / Å	(%)
1	0.114	3.394(18)	0.128(23)	3.764(33)	0.145(35)	0.094
2	0.119	3.428(15)	0.120(19)	3.759(21)	0.125(23)	0.015
3	0.135	3.443(16)	0.122(20)	3.769(20)	0.122(22)	0.009
4	0.143	3.472(17)	0.120(21)	3.775(14)	0.108(16)	0.014
5	0.181	3.501(19)	0.118(21)	3.777(14)	0.102(15)	0.039

FIGURE CAPTIONS

Figure 1. Oxygen nonstoichiometry of $Nd_2NiO_{4+\delta}$ measured using iodometric titrations. Samples were annealed under various oxygen partial pressures at 1073 K.

Figure 2. Modulus of Fourier transforms of Nd *K*-edge $k^3\chi(k)$ EXAFS of $Nd_2NiO_{4+\delta}$ annealed under various $p(O_2)$ values at 1073 K.

Figure 3. Schematic illustration of (a) coordination for Nd *K*-edge EXAFS fitting and (b) interstitial oxygen diffusion for $Nd_2NiO_{4+\delta}$. The green triangle represents the bottleneck for interstitial oxygen migration.

Figure 4. Interatomic distances of Nd-Nd1 and Nd-Nd2 bonds as a function of $p(O_2)$ for $Nd_2NiO_{4+\delta}$ annealed under various $p(O_2)$ values at 1073 K. Nd-Nd1 represents the axial coordination along the perovskite structure, while Nd-Nd2 represents the equatorial coordination.

Figure 5. (a) Oxide ionic conductivity (σ_i) and (b) oxygen surface exchange coefficient (k_O) of $Nd_2NiO_{4+\delta}$ under various $p(O_2)$ values as a function of temperature.

Figure 6. Activation energy of oxygen surface exchange coefficient (k_O) of $Nd_2NiO_{4+\delta}$ as a function of activation energy of oxide ionic conductivity (σ_i) of $Nd_2NiO_{4+\delta}$.

Figure 7. Activation energy of oxygen surface exchange coefficient and oxide ionic conductivity of $Nd_2NiO_{4+\delta}$ as a function of the bottleneck size of $Nd_2NiO_{4+\delta}$.

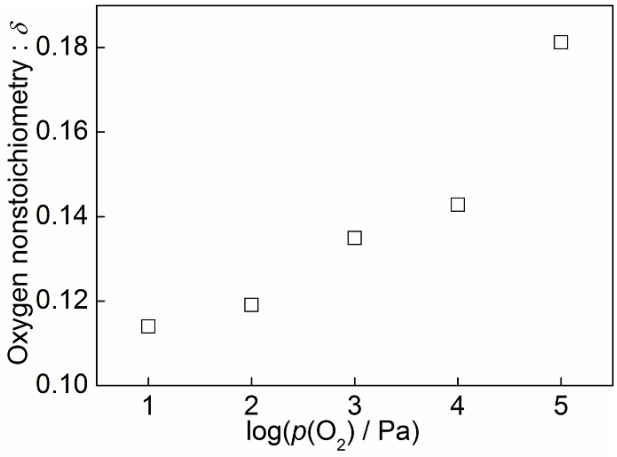

Figure 1. T. Ina et al.

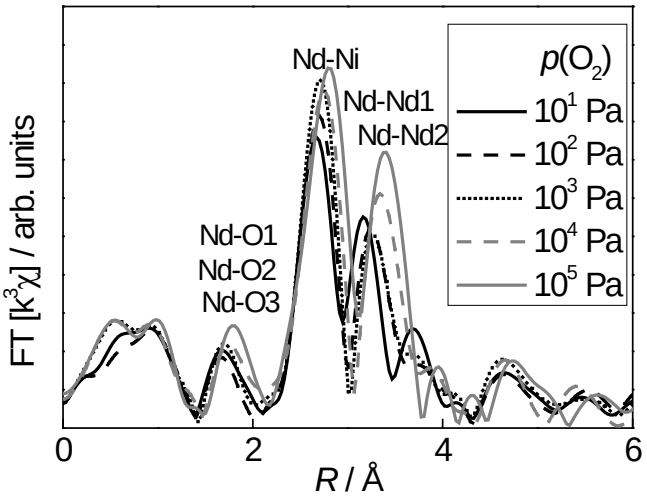

Figure 2. T. Ina et al.

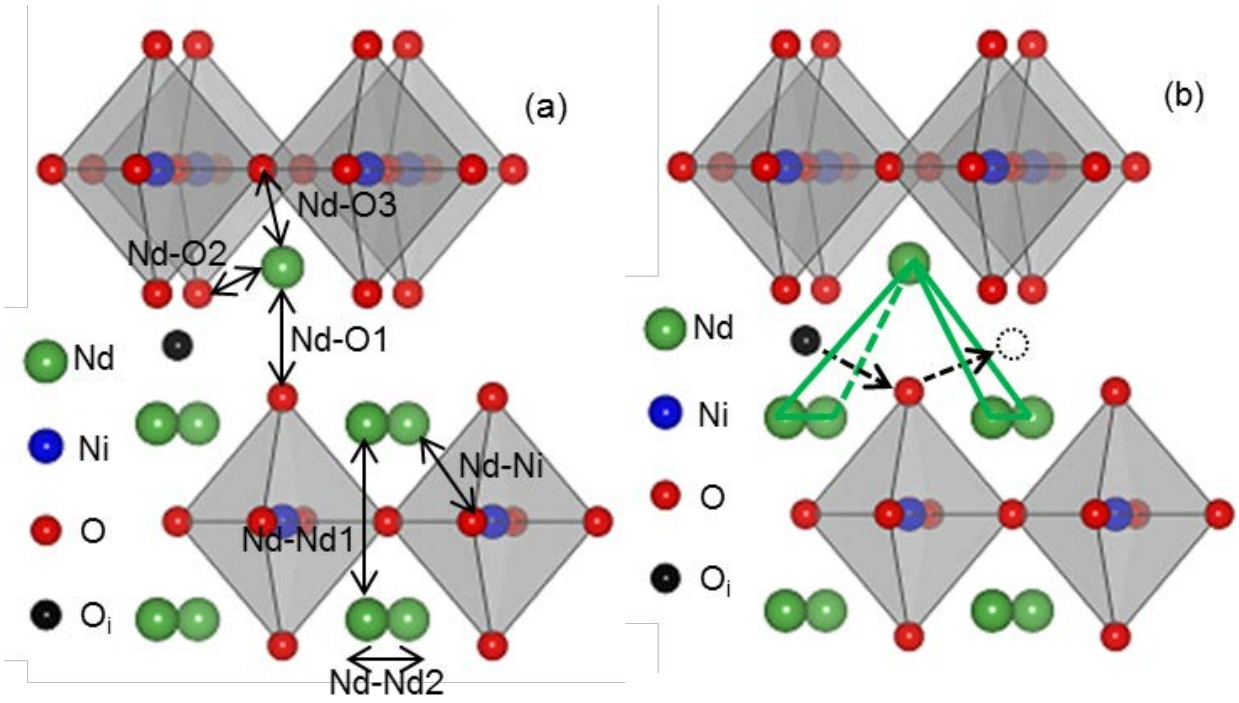

Figure 3. T. Ina et al.

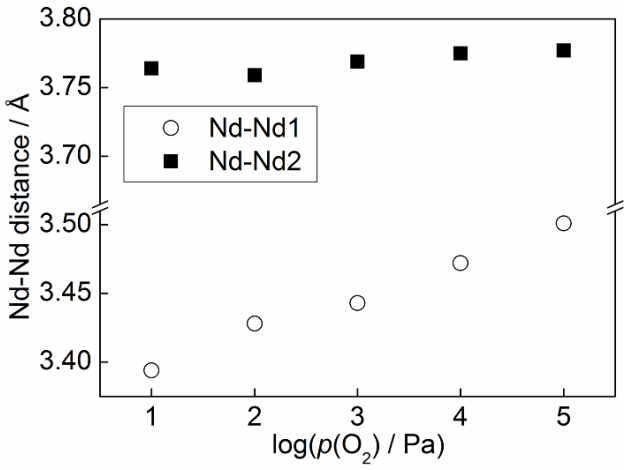

Figure 4. T. Ina et al.

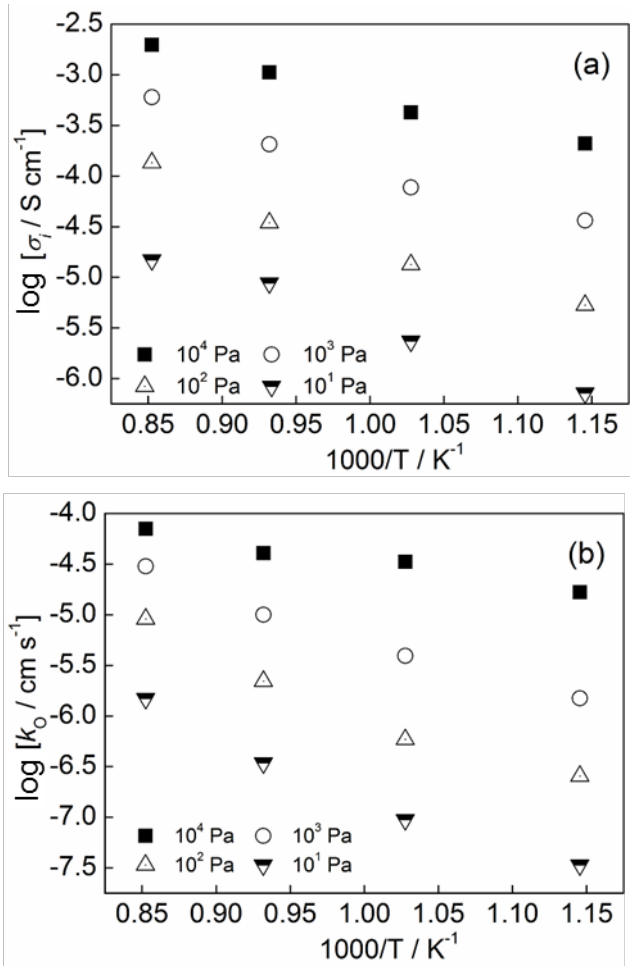

Figure 5. T. Ina et al.

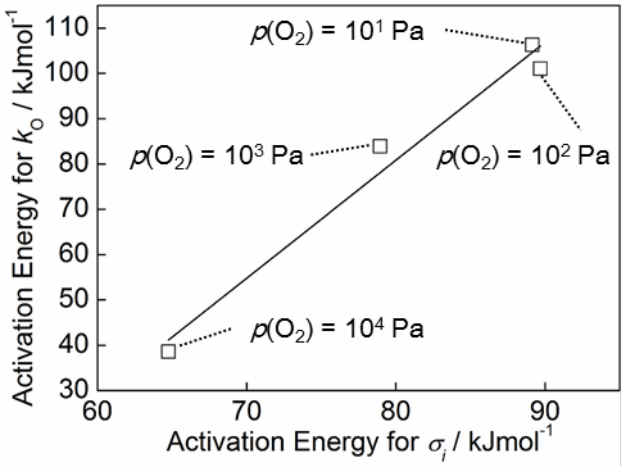

Figure 6. T. Ina et al.

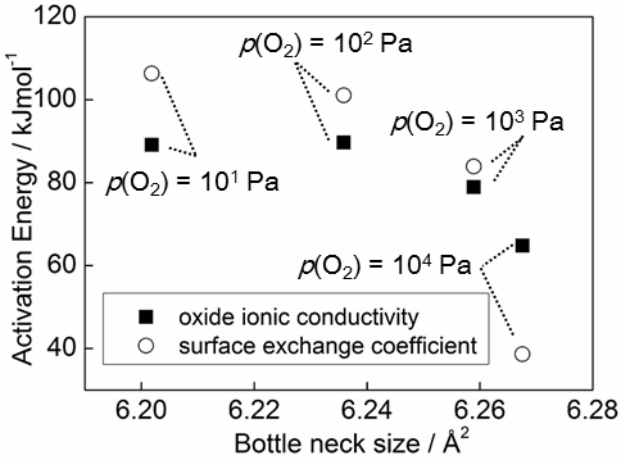

Figure 7. T. Ina et al.